Sensors and Actuators: A. Physical 335 (2022) 113384

Contents lists available at ScienceDirect

Sensors and Actuators: A. Physical

journal homepage: www.elsevier.com/locate/sna

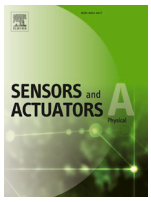

Piezoelectric benders with strain sensing electrodes: Sensor design for position control and force estimation

Rudolf Seethaler[a,*], Sepehr Zarif Mansour[a], Michael G. Ruppert[b], Andrew J. Fleming[b]

[a] University of British Columbia, Kelowna, BC V1V1V7, Canada
[b] University of Newcastle, Callaghan, NSW 2308, Australia

ARTICLE INFO

Article history:
Received 20 July 2021
Received in revised form 21 December 2021
Accepted 16 January 2022
Available online 22 January 2022

Keywords:
Piezoelectric bender
Position control
Force sensing

ABSTRACT

Piezoelectric benders are widely used in industrial applications due to their low-cost and compact size. However, due to the large relative size and cost of displacement sensors, bender actuators are often operated in open-loop or with feed-forward control, which can limit positioning accuracy to 20% of full-scale. To improve the positioning accuracy of piezoelectric benders, this article proposes integrating resistive strain gauges into the electrode surface by chemical etching or laser ablation. These strain sensors are then used to measure and control the tip displacement. The proposed sensors are shown to suffer from significant cross-coupling between the actuator voltage and measured signal; however, this can be mitigated by judicious choice of the sensor location and actuator driving scheme. In addition to position sensing, a method is also presented for simultaneous estimation of the contact force between the actuator tip and load. The proposed methods are validated experimentally by controlling the tip position of a piezoelectric bender while simultaneously estimating the force applied to a reference load cell.

1. Introduction

The low cost, compact size, and large displacement of piezoelectric bender actuators is well suited to applications such as buzzers in alarm devices, braille heads [1], needle actuators for knitting machines [2], fiber optic switches [3], positioning of hard drive heads [4], pneumatic proportional control valves [5], and cantilever detectors in atomic force microscopy (AFM) [6].

Position and force control of piezoelectric benders can be achieved by using feed-forward control using hysteresis models [7,8], charge amplifiers [9,10], or feedback control using either position self sensing [11–13] or traditional sensors such as proximity sensors, strain gauges, or laser interferometers.

Strain gauges are commonly used for estimating displacement or force in piezoelectric systems [14–17]. To save space and cost, strain gauges have also been integrated into the bender electrodes for measuring bender tip displacement. However, previous work based on strain sensors can measure the tip displacement, or contact force but not both simultaneously [18,19]. Recently, a special strain gauge geometry was proposed, whose sensitivity between strain and position is identical for excitations by tip forces and actuation voltages [20]. This allows for large tip forces when measuring displacement. This new displacement measurement can also be augmented with a simple first order model for estimating tip forces.

In this article, we develop a detailed electromechanical lumped parameter model for the strain based displacement sensor in [20]. In addition to strain response, the model also includes capacitive feedthrough from the actuation electrodes, and the induced piezoelectric voltage from the piezoelectric layer underneath the strain gauge. Thus, the model provides insights into design parameters that govern the magnitude of the unwanted feedthrough and induced piezoelectric voltage. This model will also be employed to design a position feedback controller that is robust to disturbance forces and sensor cross-coupling.

The remainder of this article is structured as follows: In Section 2, a lumped parameter model relating strain to position is developed. Section 3 outlines a simple displacement control scheme. In Section 4, the performance of the control system is experimentally verified. Finally, conclusions are provided in Section 5.

2. Modeling strain response

Two resistive strain gauges were created on the outside electrodes of a T220-A4BR-2513XB piezoelectric bender from Piezo Systems using a factory etching process. The mechanical properties are listed in Table 1. The bender is rigidly clamped at the strain gauge

* Corresponding author.
E-mail address: rudolf.seethaler@ubc.ca (R. Seethaler).

https://doi.org/10.1016/j.sna.2022.113384
0924-4247/

Table 1
Bender Specifications.

Parameter	Value
PZT Material	PZT 5A
Center Electrode Material	Brass
Bender length L_0	63.5 mm
Bender width W	31.75 mm
Bender thickness t	0.51 mm
PZT Thickness	0.19 mm
Center electrode thickness	0.13 mm
Spring constant k	0.388 N/mm
Resonant frequency f_0	88 Hz
Unclamped bender length L	57 mm
Strain gauge connector location x_1	0 mm
Strain gauge end location x_2	38 mm

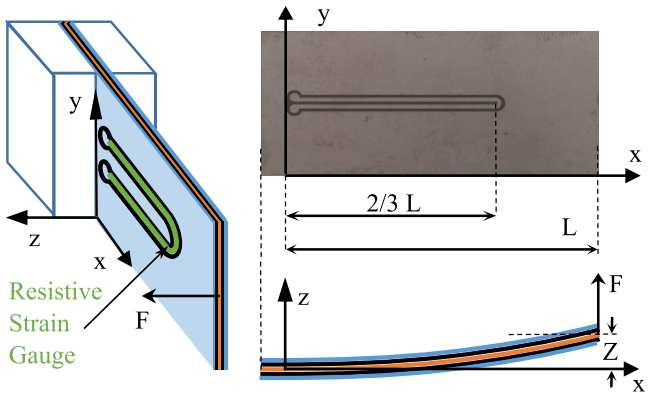

Fig. 1. Bender geometry with resistive strain gauges embedded into outside electrodes. Strain gauges span 2/3 of the bender length, which provides equal sensitivity to actuation voltage V_A and tip force F.

connectors as indicated in Fig. 1. The unclamped portion of the bender has a length of L. The bender deflects in response to a tip force F and an actuation voltage V_A applied to the outside bender electrodes. To achieve equal sensitivity between strain and tip displacement for the two excitation mechanisms, the length of the strain gauges spans two thirds of the length of the unclamped portion of the bender [20].

2.1. Sources of feedthrough

The bender consists of two piezoelectric layers (PZT 5A) which are separated by a grounded center electrode (Brass) and sandwiched between two outer electrodes (Nickel) as schematically shown in Fig. 2. This configuration reduces unwanted capacitive feedthrough from the driving voltage electrodes to the strain gauges compared to the more conventional configuration with grounded outer electrodes [19]. The remaining feedthrough is modeled as a parasitic capacitance C_F between the strain gauges and the actuation electrodes. In addition, the piezoelectric layers underneath the strain gauges will induce a voltage V_P that is coupled into the strain gauges through the piezoelectric capacitance C_P. Both of these couplings lead to significant feed through at high frequencies.

If the parasitic and piezoelectric capacitances are equal for the top and bottom layer, the unwanted feedthrough voltages can be canceled using the half bridge configuration depicted in Fig. 3. The circuit is biased with a voltage V_B and the change in strain Δ is measured by the differential bridge voltage V_S. The active strain resistors R_{S1} and R_{S2} are balanced by bridge completion resistors R_{B1} and R_{B2}. When measuring V_S, only the difference between the feedthrough components from C_{F1} and C_{F2} are seen. Similarly, only the difference between the induced piezoelectric voltages coupled into the bridge circuit through C_{P1} and C_{P2} are seen in V_S. Since the

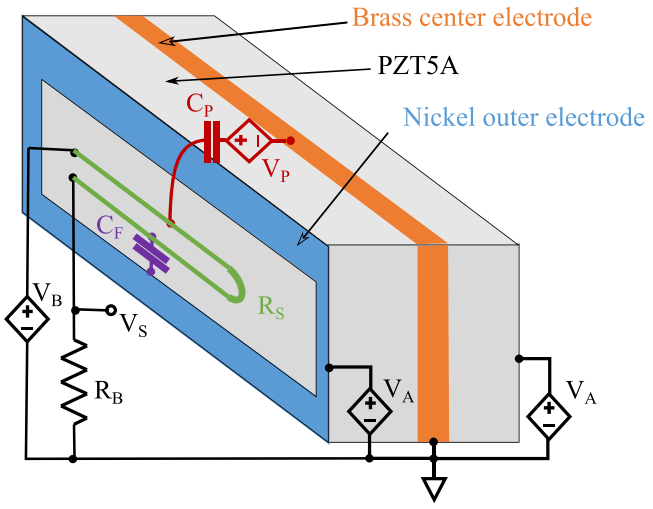

Fig. 2. Feedthrough model of the bender. Actuation voltage V_A and induced piezoelectric voltage V_P couple into the bridge voltage V_S through C_F and C_P respectively.

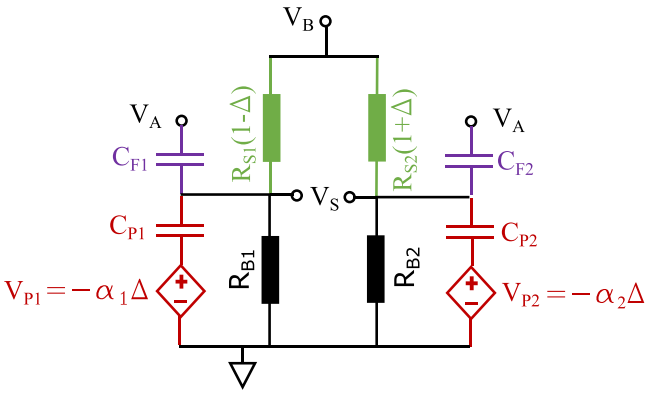

Fig. 3. Equivalent circuit diagram of Wheatstone Bridge. The active strain resistors R_{s1} and R_{s2} are balanced by bridge completion resistors R_{B1} and R_{B2}. Feedthrough from V_A and V_P distorts the bridge voltage V_S.

top and bottom layers are almost identical, the feedthrough and the induced signals are expected to be small. However, due to the capacitive coupling, these components will increase with frequency.

The capacitive nature of the feedthrough is confirmed by measuring the frequency response of tip displacement Z and bridge voltage V_S shown in Fig. 4. The measurements shown in solid lines are obtained with a Polytech PSV-Z-040 laser Doppler vibrometer. The bender is excited with a linear chirp function containing frequencies between 10 Hz and 200 Hz. Measurements are averaged over 1024 chirps to reduce noise. The narrow peak at 50 Hz is a result of the line frequency in the lab. Second order models are superimposed using dots. The tip displacement has alternating resonance poles and anti resonance zeros that correspond to the mechanical modes of the cantilever beam. The strain measurement is obtained from a custom built bridge circuit followed by a 1 Khz analog lowpass filter. It is scaled to provide the same DC-gain as the displacement Z. To separate the strain response from the feedthrough responses, the bias voltage V_B is set to zero for the red line, resulting in the response of the two feedthrough components only. The resonance peak is caused by the induced piezoelectric voltage. As expected, the feedthrough magnitude increases with frequency due to the capacitive coupling with V_S. When a biasing voltage of V_B = 2.5 V is applied, the sensor response due to tip displacement is added to V_S, leading to a flat magnitude response at low frequencies as indicated by the yellow line. However, feedthrough becomes

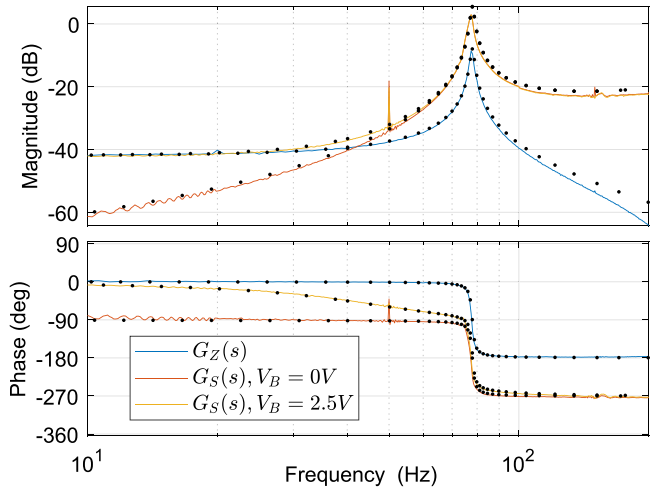

Fig. 4. Frequency responses of the piezoelectric bender. $G_Z(s)$ and $G_S(s)$ are the frequency responses measured from the actuation voltage $V_A(s)$ to the tip displacement $Z(s)$, and bridge voltage $V_S(s)$ respectively. Measurements are shown in solid lines; Second order models are superimposed using black dots. For $V_B = 0$ V, only feedthrough components are present in $V_S(s)$. When $V_B = 2.5$ V the sensor response due to tip displacement is added to the feedthrough response.

dominant well before the first resonance and drowns out strain, the actual signal of interest.

All three responses show identical resonance frequencies. However, the frequencies of the resonance zeros are unique for each measurement. The remainder of this section is dedicated to deriving a lumped parameter model that links the three responses in Fig. 4. The model will be derived for the first resonance frequency only, but could easily be extended to higher order modes by including additional poles and zeros in the transfer functions of displacement and strain. The resulting model will be used in Section 3 for designing displacement controllers.

2.2. Modeling tip deflection response $Z(s)/V_A(s)$

The transfer function from actuation voltage to tip displacement is characterized by alternating pole and zero pairs. In this study, the displacement analysis is limited to a dominant single pole pair:

$$G_Z(s) = \frac{Z(s)}{V_A(s)} = \frac{K_Z}{(\frac{s}{\omega_n})^2 + \frac{2\zeta s}{\omega_n} + 1} \tag{1}$$

where ω_n, ζ, and K_Z are the natural frequency, damping ratio, and DC gain respectively. The lowest resonance frequency of a bender is caused by the first bending mode. It can be determined analytically from [21]:

$$\omega_n = 3.52\sqrt{\frac{EIL^3}{m}} \tag{2}$$

where E, I, L, and m are the Young's modulus, the second moment of area, the length of the beam, and the mass of the beam. The bender in this study has a natural frequency of 78 Hz with a damping ratio of $\zeta = 0.01$. The DC gain of the bender is $K_z = 0.008$ mm/V. This model fits the measurements in Fig. 4 well and for comparison it is superimposed on the measurement using black dots.

2.3. Modeling the bridge voltage response $V_S(s)/V_A(s)$

The deflection of the bender is accompanied by strain in the top and bottom layer. This strain is detected by the resistive strain gauges etched into the electrodes. The transfer function between applied voltage and measured average strain along the strain gauge, $\Delta(s)$, has the same poles as the deflection transfer function, but a different DC gain, K_Δ. That is, the transfer function from applied voltage to strain is

$$G_\Delta(s) = \frac{\Delta(s)}{V_A(s)} = \frac{K_\Delta}{\left(\frac{s}{\omega_n}\right)^2 + \frac{2\zeta s}{\omega_n} + 1}. \tag{3}$$

The strain, $\Delta(s)$, is transformed to a measurable bridge voltage $V_S(s)$ using the bridge circuit shown in Fig. 3. Unfortunately, the induced piezoelectric voltage $V_P(s)$ and the actuation voltage $V_A(s)$ are also coupled into $V_S(s)$. An expression relating bridge voltage $V_S(s)$ to actuation voltage $V_A(s)$ is derived in the Appendix and is found to be:

$$G_S(s) = \frac{V_S(s)}{V_A(s)} = \frac{K_S}{2}(Cs + G_\Delta(s)(V_B - \alpha s)). \tag{4}$$

The difference in parasitic capacitance between top and bottom layer causes a feed-trough from the actuation voltage that is described by C. The difference in induced piezoelectric voltage is characterized by α. Both of these parameters are obtained by fitting (4) to the experimental response of V_S to excitations from the actuation voltage V_A. The gain K_S is introduced to adjust the scale of the bridge voltage. The DC magnitude of the bridge voltage is adjusted to match the DC magnitude of the tip deflection:

$$K_S = \frac{2K_Z}{K_\Delta V_B}. \tag{5}$$

The fitted second order models in Fig. 3 correspond well to the measurements. However, the negative sign of the induced piezoelectric voltage results in a dominant pair of non-minimum phase zeros whose frequency is well below the first resonance frequency. This is shown graphically with the pole zero map in Fig. 5, where the zero locations of $\frac{V_S(s)}{V_A(s)}$ are plotted for three values of V_B that represent the typical range of bridge bias voltages for commercial strain gauges.

Non-minimum phase zeros in the plant transfer function reduce the stability margins of closed loop control systems. Since it is not possible to invert a plant with non-minimum phase zeros, these ultimately limit the bandwidth of a closed loop controller. Unfortunately, the presence of these non-minimum phase zeros is difficult to avoid. They are the result of geometry and material variations between the top and bottom layer strain gauges. Fig. 5 illustrates that increasing the bridge bias voltage V_B increases the frequencies of the non-minimum phase zeros towards the first resonance frequency. However, the resulting higher current through

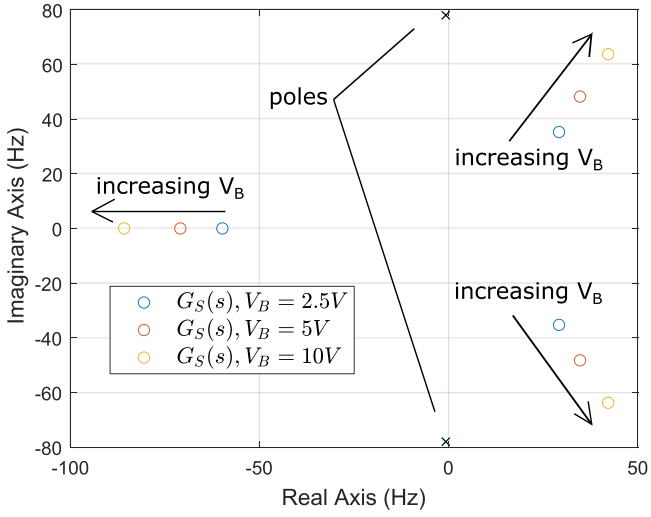

Fig. 5. Pole zero map of $G_S(s) = V_S(s)/V_A(s)$. The frequency of non-minimum phase zeros increases with bridge bias voltage V_B. The location of the lightly damped poles at 78 Hz is unaffected by the magnitude of V_B.

the strain gauges dissipates more heat. Any resistance differential of the two strain gauges would then lead to a temperature difference between top and bottom electrodes and drift in the strain measurement.

2.4. Modeling contact force, F_C

From the previous section, a position controller that uses etched strain gauges for position feedback is limited by the non-minimum phase zeros below the first resonance frequency. Thus, a model for estimating contact forces at the tip of the bender can be quasi static as the effect of inertial forces is negligible. By also neglecting hysteresis, a simple linear model for contact force F_C is ([22]):

$$F_C = nV_A - kZ \tag{6}$$

where n is a piezoelectric coupling parameter, k is the bender stiffness, and the tip displacement Z is estimated from the strain sensor. Both n and k are fitting parameters obtained from fitting the model (6) to the experimental data. Even though the lack of a hysteresis term in this model leads to force estimation errors of 10%, this simplification is sufficient for many practical applications ([20]).

3. Controller design

Pick and place operations for bender type actuators typically require step position changes. An ideal transient response between steps should minimize settling time and overshoot.

A block diagram of the position control system in this study is shown in Fig. 6. The plant consists of a transfer function for displacement, $G_Z(s)$, and a transfer function for the bridge voltage $G_S(s)$. The controller bandwidth is limited by the dominant non-minimum phase zeros of $G_S(s)$. Since $G_S(s)$ shares the same DC gain and dominant pole pair with $G_Z(s)$ (see Figure Fig. 4), controlling the bridge voltage $V_S(s)$ will also control bender position $Z(s)$. The two signals will differ during transients but they will approach each other during steady state.

The bode plot of the plant transfer function $G_S(s)$ shown in yellow in Fig. 1 illustrates the rising magnitude response with frequency that is a result of feedthrough from $V_A(s)$ and the induced piezoelectric voltage $V_P(s)$. This causes instability due to positive feedback at high frequencies when using a simple proportional feedback controller. An integral controller stabilizes the control loop:

$$C_I(s) = \frac{K_I}{s}. \tag{7}$$

However, the simple integral controller leads to a slow closed loop response since the resonance peak limits the loop gain K_I required to achieve sufficient phase margin. Adding a notch filter in series with the integral controller allows for higher loop gain which results in a faster closed loop response:

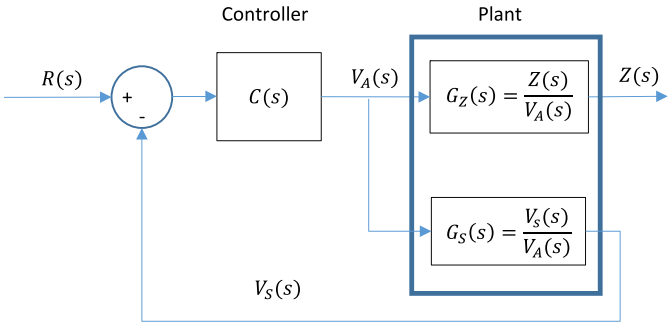

Fig. 6. Position control loop. $G_Z(s)$ and $G_S(s)$ share the same poles but they have different zeros.

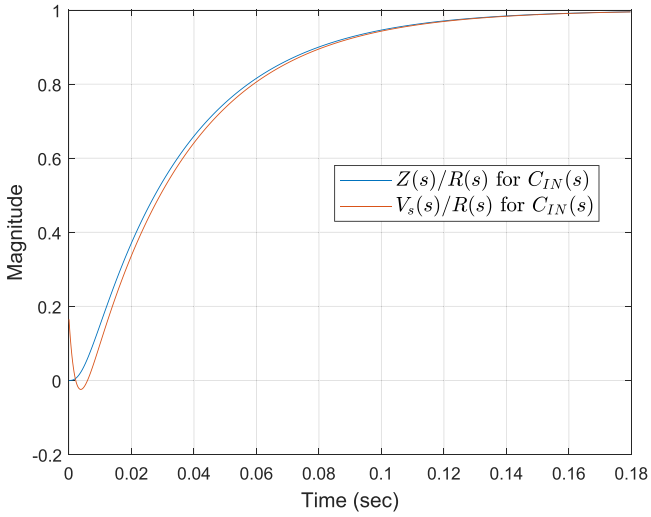

Fig. 7. Modeled closed loop step response with 20 dB gain margin. Bridge voltage V_S and tip displacement Z have a time constant of approximately 0.05 s.

$$C_{IN}(s) = \frac{K_I}{s}\frac{s^2 + 2\zeta\omega_n s + \omega_n^2}{s^2 + 2\omega_n s + \omega_n^2}. \tag{8}$$

In an atomic force microscope with a bender tapping a sample, the contact of the bender tip with the sample would increase the resonance frequency. If the bender were used in a micro gripper, the added mass of an object being held by the gripper would reduce the resonance frequency. Thus, in a practical application it can be necessary to widen the stop band of the notch filter in order to ensure sufficient damping for the expected range of resonance frequencies. Fig. 7 illustrates the modeled step response of the integral controller and notch filter with a 20 dB gain margin. The transient responses of $V_S(s)/R(s)$ and $Z(s)/R(s)$ differ slightly due to different zero locations, but they approach the same final value with a time constant of approximately 0.05 s

4. Experimental validation

The performance of the position controller is evaluated experimentally using the setup shown in Fig. 8. A MicroLabBox from dSpace is utilized to perform data acquisition and control. It is connected to the strain gauge on the bender through a custom bridge circuit and a Krohn-Hite 3384 anti aliasing filter. The control voltage is amplified by a PiezoDrive PD200 amplifier and then

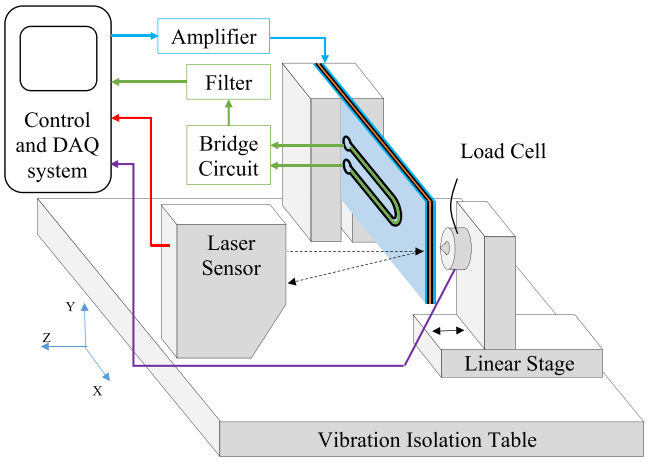

Fig. 8. Experimental setup. The position of the loadcell can be adjusted to provide different levels of contact force.

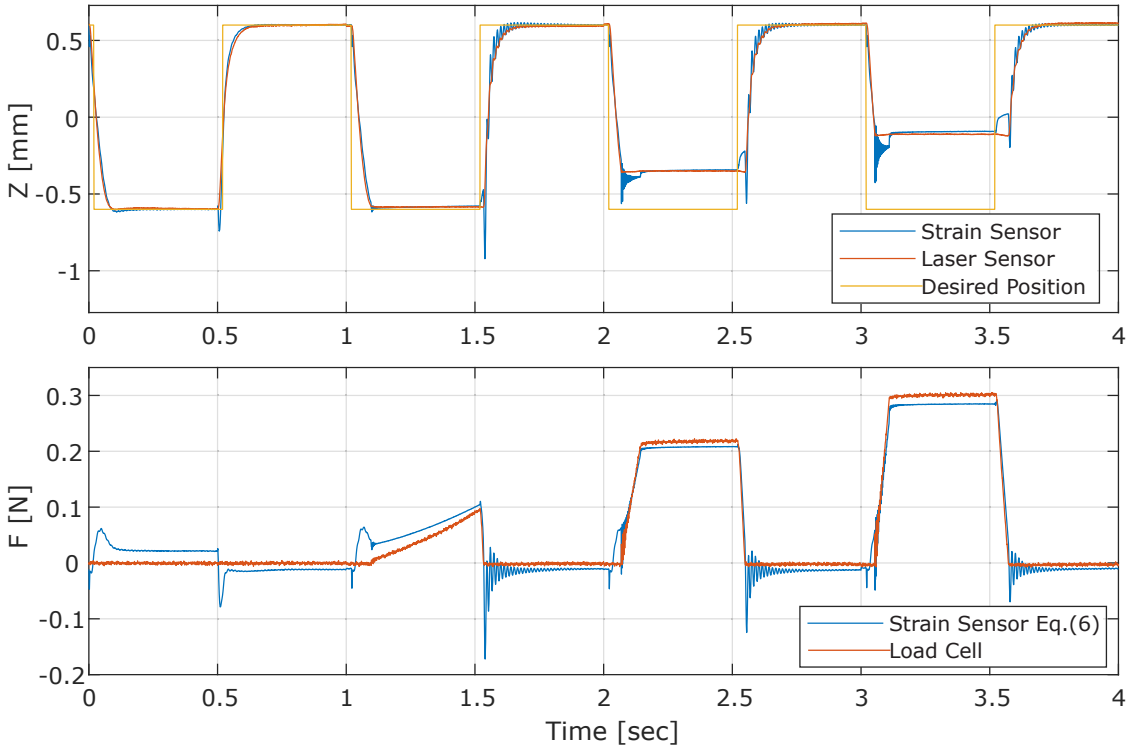

Fig. 9. Experimental step response with blocking forces. The bender is driven against a load cell. The load cell is stationary during contact, but is moved closer each cycle.

applied to the bender electrodes. A Di-Soric LAT61 Laser triangulation sensor with a resolution of 1.5 μm and a bandwidth of 2.5 kHz is also connected to the MicroLabBox. The laser sensor is not utilized by the control system but provides a ground truth for evaluating the accuracy of the strain sensor. To study the effect of disturbance forces, a Forsentek FC10C-5 kg strain based load cell with a maximum load rating of 5 kg is positioned relative to the tip of the bender with a single axis positioning stage from Thorlabs.

During the experiments, the bender is tasked to follow cyclic step changes between ± 0.6 mm which represents approximately 75% of the bender's displacement range. During the first cycle, no disturbance forces are present. During each subsequent cycle, the load cell is moved closer to the bender leading to progressively larger disturbance forces.

Displacement and force are shown in rows one and two of Fig. 9 respectively. During transients, the difference between the strain sensor and the laser sensor increases, but they approach each other during steady state. This is a result of the feedthrough components that are present in the strain measurements but absent in the laser measurements. During steady state, the position measurement error drops to less than 2% even in the presence of considerable disturbance forces, that are caused by the load cell blocking the bender's tip displacement in cycles two, three, and four.

The second row of Fig. 9 compares the tip force measured by the reference load cell to the tip force estimate obtained from (6). The large transient oscillations seen in the latter measurement originate from the strain based position measurement feeding into (6). The resulting transient force measurement errors can reach up to 80% of full scale when the bender looses contact with the load cell as seen at 1.5 s. Furthermore, since the force estimation does not take into account hysteresis, errors of up to 10% are observed during the quasi static portions of the experiment. This error could be improved by adding a hysteresis model, but this is not the focus of the current study since most pick and place operations only require rough estimates of force.

5. Conclusions

This article describes a position controller for a piezoelectric bender with strain gauges etched into the outer electrodes. A lumped parameter model reveals that the strain measurements are dominated by a pair of non-minimum phase zeros at a frequency slightly lower than the first mechanical resonance frequency of the bender. Thus, the bandwidth of the position controller is limited by the frequency of the non-minimum phase zeros. Nevertheless, step responses with a time constant of approximately 50 ms and steady state errors of less than 2% are achieved experimentally. A linear model for estimating contact forces is also presented and results in less than 10% error. Given the promising results in this study, the authors will expand the control scheme to a setup with two benders that can perform simultaneous force and position control for an object held between the benders' tips.

CRediT authorship contribution statement

Rudolf Seethaler: Conceptualization, Methodology, Investigation, Writing – original draft. **Sepehr Zarif Mansour:** Writing – review & editing. **Michael G. Ruppert:** Conceptualization, Methodology, Validation, Writing – review & editing. **Andrew J. Fleming:** Conceptualization, Resources, Writing – review & editing.

Declaration of Competing Interest

The authors declare that they have no known competing financial interests or personal relationships that could have appeared to influence the work reported in this paper.

Appendix A. Appendix: Derivation of the Expression for Bridge Voltage

The transfer function between actuation voltage $V_A(s)$ and bridge voltage $V_S(s)$ is derived from Fig. 3. The superposition theorem is applied to include piezoelectric voltage $V_P(s)$ and feedthrough from the actuation voltage $V_A(s)$. We first analyze the resistance change of the strain gauge $R(1+\Delta(s))$. In this case, the response from capacitive feedthrough and induced piezoelectric voltage are removed by setting $V_A(s)$, $V_{P1}(s)$, and $V_{P2}(s)$ to zero. Further, assuming perfectly matched parameter values between the four bridge branches ($R = R_{S1} = R_{S2} = R_{B1} = R_{B2}$, $C_F = C_{F1} = C_{F2}$, and $C_P = C_{P1} = C_{P2}$) the bridge voltage $V_S(s)$ is described as a function of the changes in strain $\Delta(s)$ of the strain gauges:

$$\left.\frac{V_S(s)}{\Delta(s)}\right|_{\substack{V_A=0\\V_{P1}=0\\V_{P2}=0}} = \frac{V_B}{2}\frac{2s+\omega_b^2}{(s+\omega_b)^2} \tag{9}$$

where $\omega_b = \frac{2}{R(C_F+C_P)}$. The scale factor of $V_B/2$ is a result of the half bridge configuration employed in this setup. The lead and quadratic lag term are a result of the coupling capacitances C_F and C_P.

For perfectly matched parameters between the two piezoelectric layers, the bridge configuration results in a complete cancellation of feedthrough originating from $V_A(s)$, $V_{P1}(s)$, and $V_{P2}(s)$. In practice, this cannot be achieved.

We will first study the effect of actuator feedthrough caused by an imbalance between C_{F1} and C_{F2}. By setting V_B, $V_{P1}(s)$, and $V_{P2}(s)$ to zero, the transfer function between $V_S(s)$ and $V_A(s)$ is obtained:

$$\left.\frac{V_S(s)}{V_A(s)}\right|_{\substack{V_B=0\\V_{P1}=0\\V_{P2}=0}} = \frac{C_{F1}-C_{F2}}{2}\frac{\omega_b s}{\omega_b+s}. \tag{10}$$

Modeling the induced piezoelectric voltage proportional to strain, $V_{P1}(s) = -\alpha_1\Delta(s)$ and $V_{P2}(s) = -\alpha_2\Delta(s)$, the transfer function between $V_S(s)$ and strain $\Delta(s)$ due to the induced piezoelectric voltages is derived as

$$\left.\frac{V_S(s)}{\Delta(s)}\right|_{\substack{V_A=0\\V_B=0}} = -\frac{C_{P1}\alpha_1-C_{P2}\alpha_2}{2}\frac{\omega_b s}{\omega_b+s}. \tag{11}$$

In practice, ω_b is much larger than the frequencies of the non-minimum phase zeros of $G_S(s)$. Since the controller bandwidth is limited by these non-minimum phase zeros, (9), (10), and (11) can be combined into a compact transfer function of the bridge voltage $V_S(s)$ over actuation voltage $V_A(s)$:

$$G_S(s) = \frac{V_S(s)}{V_A(s)} = \frac{1}{2}(Cs + G_\Delta(s)(V_B - \alpha s)) \tag{12}$$

where $C = C_{F1} - C_{F2}$ and $\alpha = C_{P1}\alpha_1 - C_{P2}\alpha_2$.

References

[1] P. Smithmaitrie, J. Kanjantoe, P. Tandayya, Touching force response of the piezoelectric Braille cell, Disability and rehabilitation, Assist. Technol. 3 (6) (2008) 360–365, https://doi.org/10.1080/17483100802281442

[2] K. Mista, Warp knitting machine with Jacquard-control, 1993. https://patents.google.com/patent/EP0583631A1/en.

[3] H. J. Ramsey, M. L. Dakss, Piezoelectric optical switch, 1979. https://patents.google.com/patent/US4303302/en.

[4] K.W. Chan, W.-h. Liao, Precision positioning of hard disk drives using piezoelectric actuators with passive damping, 2006 Int. Conf. Mechatron. Autom. (2006) 1269–1274, https://doi.org/10.1109/ICMA.2006.257809

[5] White paper piezo technology in pneumatic valves, Tech. rep., Festo AG & Co KG, 2017.

[6] M.G. Ruppert, S.I. Moore, M. Zawierta, A.J. Fleming, G. Putrino, Y.K. Yong, Multimodal atomic force microscopy with optimized higher eigenmode sensitivity using on-chip piezoelectric actuation and sensing, Nanotechnology 30 (8) (2019) 085503.

[7] B. Mokaberi, A.A. Requicha, Compensation of scanner creep and hysteresis for afm nanomanipulation, IEEE Trans. Autom. Sci. Eng. 5 (2) (2008) 197–206.

[8] M. Rakotondrabe, Bouc-Wen modeling and inverse multiplicative structure to compensate hysteresis nonlinearity in piezoelectric actuators, IEEE Trans. Autom. Sci. Eng. 8 (2) (2011) 428–431, https://doi.org/10.1109/TASE.2010.2081979

[9] K. Furutani, M. Urushibata, N. Mohri, Improvement of control method for piezoelectric actuator by combining induced charge feedback with inverse transfer function compensation, Proc. 1998 IEEE Int. Conf. Robot. Autom. 2 (1998) 1504–1509, https://doi.org/10.1109/ROBOT.1998.677325

[10] A.J. Fleming, S.O.R. Moheimani, A grounded-load charge amplifier for reducing hysteresis in piezoelectric tube scanners, Rev. Sci. Instrum. 76 (2005), https://doi.org/10.1063/1.1938952

[11] M.G. Ruppert, S.R. Moheimani, High-bandwidth multimode self-sensing in bimodal atomic force microscopy, Beilstein J. Nanotechnol. 7 (1) (2016) 284–295.

[12] M. Rakotondrabe, I.A. Ivan, S. Khadraoui, P. Lutz, N. Chaillet, Simultaneous displacement/force self-sensing in piezoelectric actuators and applications to robust control, IEEE/ASME Trans. Mechatron. 20 (2) (2015) 519–531, https://doi.org/10.1109/TMECH.2014.2300333

[13] M.N. Islam, R.J. Seethaler, Sensorless position control for piezoelectric actuators using a hybrid position observer, IEEE/ASME Trans. Mechatron. 19 (2) (2014) 667–675, https://doi.org/10.1109/TMECH.2013.2250990

[14] F. Arai, A. Kawaji, T. Sugiyama, Y. Onomura, M. Ogawa, T. Fukuda, H. Iwata, K. Itoigawa, 3D micromanipulation system under microscope, MHA'98. Proc. 1998 Int. Symp. . Micro Hum. Sci. (1998) 127–134, https://doi.org/10.1109/MHS.1998.745764

[15] A. Menciassi, A. Eisinberg, M. Carrozza, P. Dario, Force sensing microinstrument for measuring tissue properties and pulse in microsurgery, IEEE/ASME Trans. Mechatron. 8 (1) (2003) 10–17, https://doi.org/10.1109/TMECH.2003.809153

[16] M. Goldfarb, N. Celanovic, A flexure-based gripper for small-scale manipulation, Robotica 17 (2) (1999) 181–187, https://doi.org/10.1017/S026357479900096X

[17] P. Rougeot, A. Mohand-Ousaid, D. Gendreau, M. Hammouche, M. Rakotondrabe, Design, modeling and simulation of a three-layer piezoelectric cantilevered actuator with collocated sensor, Sens. -Gener. Robot. III 9859 (2016) 98590F.

[18] D. Campolo, R. Sahai, R. Fearing, Development of piezoelectric bending actuators with embedded piezoelectric sensors for micromechanical flapping mechanisms, IEEE Int. Conf. Robot. Autom. 3 (2003) 3339–3346, https://doi.org/10.1109/ROBOT.2003.1242106

[19] S. ZarifMansour, R.J. Seethaler, Y.R. Teo, Y.K. Yong, A.J. Fleming, Piezoelectric bimorph actuator with integrated strain sensing electrodes, IEEE Sens. J. 18 (14) (2018) 5812–5817, https://doi.org/10.1109/JSEN.2018.2842138

[20] R. Seethaler, S.Z. Mansour, M.G. Ruppert, A.J. Fleming, Position and force sensing using strain gauges integrated into piezoelectric bender electrodes, Sens. Actuators A: Phys. 321 (2021) 112416, https://doi.org/10.1016/j.sna.2020.112416 ⟨https://www.sciencedirect.com/science/article/pii/S0924424720317325⟩.

[21] R. Blevins, Formulas for Natural Frequency and Mode Shape, Krieger Publishing, Malabar, Fl, USA, 2001.

[22] M. Goldfarb, N. Celanovic, A lumped parameter electromechanical model for describing the nonlinear behavior of piezoelectric actuators, J. Dyn. Syst., Meas., Control 119 (3) (1997) 478–485, https://doi.org/10.1115/1.2801282

Rudolf J. Seethaler: (M'07) received the B.Sc. degree in mechanical engineering at the university of Toronto, Canada, in 1991 and the Ph.D. degree in mechanical engineering from the University of British Columbia (UBC), Vancouver, BC, Canada, in 1997. From 1997–2005, he was a Senior Controls Engineer at BMW AG, Munich, Germany. He is currently an Associate Professor with UBC. His research interests include the design and control of high-speed motion control systems, and the optimization of

manufacturing processes.

Sepehr Zarif Mansour: received the Bachelor's of Applied Science degree in mechanical engineering from the University of Tehran, Tehran, Iran, in 2013, and the PhD degree in mechanical engineering with the University of British Columbia, Kelowna, BC, Canada, in 2019. He is currently working at MDI Canada, Toronto, Canada as a researcher. His research interests include the design and control of high-speed motion control systems for space applications.

Michael G. Ruppert: received the Dipl.-Ing. degree in automation technology from the University of Stuttgart, Germany, in 2013 and the PhD degree in Electrical Engineering from The University of Newcastle, Australia in 2017. As a visiting researcher, he was with The University of Texas at Dallas, USA from 2015 until 2016 and he is currently a postdoctoral research fellow at The University of Newcastle. His research interests include the utilization of system theoretic tools for sensing, estimation and control in high-speed and multifrequency atomic force microscopy.Dr Ruppert's research has been recognized with the 2019 Best Conference Paper Award at the 2019 International Conference on Manipulation, Automation and Robotics at Small Scales (MARSS), the 2018 IEEE Transactions on Control Systems Technology Outstanding Paper Award, and the 2017 University of Newcastle Higher Degree by Research Excellence Award.

Andrew J. Fleming: (M′02) received the B.Sc. degree in electrical engineering and the Ph.D. degree in mechatronics engineering from the University of New-castle, Callaghan, NSW, Australia, in 2000 and 2004, respectively. He is currently an Australian Research Council Future Fellow and the Director with the Precision Mechatronics Lab, University of Newcastle. He is the co-author of three books, and more than 180 journal and conference articles. He is the Inventor of several patent applications. His research interests include lithography, nano positioning, scanning probe microscopy, and biomedical devices. Dr. Fleming received the Academy for Technological Sciences and Engineering Baterham Medal in 2016, the Newcastle Innovation Rising Star Award for Excellence in Industrial Engagement in 2012, the IEEE Control Systems Society Outstanding Paper Award in 2007, and the University of Newcastle Researcher of the Year Award in 2007.